Effect of charge compensation on the photoelectrochemical properties of Ho-doped SrTiO3 films

Long Zhao, Liang Fang, Wen Dong, Fengang Zheng, Mingrong Shen, and Tom Wu

---

Articles you may be interested in

Control of VO••~TiTi′ dipole pairs as well as MgTi″ defects on dielectric properties of Mg doped (Pb0.35Sr0.65)TiO3 thin film
J. Appl. Phys. **119**, 014103 (2016); 10.1063/1.4939589

Influence of charge compensation mechanisms on the sheet electron density at conducting LaAlO3/SrTiO3-interfaces
Appl. Phys. Lett. **100**, 052103 (2012); 10.1063/1.3679139

Surface functionalized Ba 0.6 Sr 0.4 TiO 3 /poly(vinylidene fluoride) nanocomposites with significantly enhanced dielectric properties
Appl. Phys. Lett. **95**, 202904 (2009); 10.1063/1.3257371

Microstructure and electrical properties of Ho-doped BaTiO 3 -sputtered films
J. Appl. Phys. **98**, 026109 (2005); 10.1063/1.1984083

Positive temperature coefficient of resistivity in Pt∕(Ba 0.7 Sr 0.3) TiO 3∕YBa 2 Cu 3 O 7 - x capacitors
Appl. Phys. Lett. **85**, 5019 (2004); 10.1063/1.1827928

Effect of charge compensation on the photoelectrochemical properties of Ho-doped SrTiO$_3$ films

Long Zhao,[1] Liang Fang,[1,a)] Wen Dong,[1] Fengang Zheng,[1] Mingrong Shen,[1] and Tom Wu[2]

[1]*Jiangsu Key Laboratory of Thin Films and Department of Physics, Soochow University, Suzhou 215006, People's Republic of China*
[2]*Division of Physics and Applied Physics, School of Physical and Mathematical Sciences, Nanyang Technological University, Singapore 637371, Singapore*

When Ho^{3+} ions are substituted at Sr^{2+} sites in SrTiO$_3$ (STO), the excess positive charges are compensated via three complementary routes: (1) strontium vacancies, (2) titanium vacancies, and (3) conduction electrons. In this study, we show that the photoelectrochemical properties of Ho-doped STO films are dependent on the charge compensation mechanisms. The compensation mechanism via the titanium vacancies exhibits the highest photocurrent density, which is 1.7 times higher than that of the pure STO sample. Based on the measured dielectric properties and electrochemical impedance spectroscopy data, we propose that the enhanced dielectric constant of the films can enlarge the width of the space charge region at the film/liquid interface, which eventually leads to the increase of the photocurrent density. Further enhancement of photocurrent density is obtained in the samples decorated with appropriate amounts of Pt nanoparticles, showing the advantage of composites for achieving the efficient photoelectrochemical property. © 2013 American Institute of Physics. [http://dx.doi.org/10.1063/1.4798829]

Perovskite-structured oxides (ABO$_3$) have been widely studied for a long time because of their versatile dielectric, ferroelectric, ferromagnetic, and even superconducting properties. As one of most studied materials, SrTiO$_3$ (STO) is classified as quantum paraelectric and possesses a highly polarizable lattice at room temperature.[1] With cooling, the dielectric permittivity of STO increases monotonously and levels off without any dielectric peak, indicating that the ferroelectric transition is suppressed by the large quantum fluctuations. In addition, the dielectric property of STO is very sensitive to extrinsic factors such as defects, impurities, strains, and applied electric fields.[2–4] For example, the A-site substitution of Sr^{2+} by isovalent or heterovalent ions (e.g., Ba^{2+}, Pb^{2+}, and Bi$^+$) can induce ferroelectricity and intermediate glass- or relaxor-like states.[5–7]

Besides electronic applications, STO is also regarded as an effective photocatalytic material for photoelectrochemical (PEC) water splitting.[8] So far, a myriad of semiconductor photoelectrodes, such as N-doped TiO$_2$,[9] WO$_3$,[10] Fe$_2$O$_3$,[11] and BiVO$_4$,[12] have been investigated for water splitting. However, most of them have to photooxidize water in the presence of an electrical or chemical bias due to the fact that their space charge layers are not effective for separating electron-hole pairs and avoiding charge recombination. Although the intrinsic STO is an n-type semiconductor with a large band gap of 3.2 eV, it can still decompose H$_2$O into H$_2$ and O$_2$ without applying an external bias potential because its conduction band level is higher than the redox potential for the H$_2$ evolution.[13] For instance, under the UV irradiation, NiO$_x$–STO has been shown to photolyze water into H$_2$ (up to 100 mmol g^{-1} h^{-1}) and stoichiometric O$_2$.[14] Moreover, STO also has excellent thermal stability, photo-corrosion resistability, and good structural stability during the water splitting process.

In order to further improve the PEC property, many efforts have been made to investigate the cation-doped STO. For example, Irie *et al.* reported that Pb^{2+} substitution on the Sr^{2+} sites could extend the absorption edge of STO powders from UV to visible light region.[15] Kudo *et al.* recently reported that STO powders with Rh^{4+} doped at Ti^{4+} sites showed a cathodic photocurrent under the visible light irradiation.[16] Apart from isovalent cations, trivalent rare earth (RE^{3+}) cations also have a strong influence on the PEC property of STO. Shi *et al.* have studied STO powders doped with Er^{3+} ions at different sites,[17] and they found that in the presence of sacrificial reagents, the Er^{3+} doped STO samples with the B-site occupancy showed better PEC performance than that with the A-site occupancy in the visible-light-driven H$_2$ and O$_2$ evolution. They suggested that such a phenomenon could be attributed to the stronger local internal field resulting from the Er^{3+} ions with the B-site occupancy.

In addition, unlike the isovalent ion doping, another unique feature of the RE^{3+}-doped STO is the rich and different charge compensation mechanisms induced by doping.[18] In general, when RE^{3+} ions are incorporated at the Sr^{2+} sites, the excess positive charges can be compensated by either strontium vacancy (V$_{Sr}$), titanium vacancy (V$_{Ti}$), or simply conduction electron (e).[19] Since the charge balance is an important factor dictating the PEC properties of photocatalysts,[20] it is natural to ask whether there is a connection between the charge compensation mechanism and the PEC properties of RE^{3+}-doped STO. So far, it remains an open question. Moreover, powder photocatalyst is often used in PEC applications to achieve high surface areas and to simplify synthesis, but powder photocatalyst itself is difficult to retrieve, and it is also not possible to investigate the effect of photocarrier dynamics in the powder form.[21] In contrast, PEC systems in the thin film form overcome these disadvantages, and thus they can be readily extended to industrial applications.

a)Electronic mail: lfang@suda.edu.cn.

In this study, PEC cells consisting of Ho-doped STO nanoscale films were fabricated by the sol-gel method. Focusing on the effect of Ho^{3+} substitution at the Sr^{2+} sites, we found that the photocurrent density of the Ho-doped STO samples is strongly dependent on the charge compensation mechanism. Contrary to the general belief, the maximum in the photocurrent density is associated with an anomalously high dielectric constant that leads to an enlarged space charge region. In addition, Pt nanoparticles were subsequently deposited onto the films, which further enhanced the photocurrent density. This study provides a new approach to enhance the PEC properties of STO and particularly demonstrates the important role of dielectric properties of such oxides in determining the PEC performance.

The ionic radius of Ho^{3+} is 1.23 Å, which is close to that of Sr^{2+} (1.44 Å), but much larger than that of Ti^{4+} (0.605 Å), leading to a preferential A-site doping of Ho in STO.[22] Experimentally, sol-gel precursors of Sr, Ti, and Ho with different molar ratios were used, and the corresponding chemical formulas of the Ho-doped STO films are $Sr_{1-3x/2}Ho_xTiO_3$ (STO-V_{Sr}, strontium vacancy compensation), $Sr_{1-x}Ho_xTi_{1-x/4}O_3$ (STO-V_{Ti}, titanium vacancy compensation), and $Sr_{1-x}Ho_x$ $(Ti_{1-x}^{4+}Ti_{1-x}^{3+})O_3$ (STO-e, conduction electron compensation), where x is fixed at 2.5 mol. %. It should be noted that in A-site-doped STO, the solubility limits for La^{3+} and Y^{3+} ions are 20% and 4%, respectively.[23] Since the radius of Ho^{3+} ions is between those of La^{3+} and Y^{3+} ions, the solubility limit of Ho is expected to be in the range of 4%–20%, which is much higher than the doping level in our samples. Moreover, the sol gel synthesis method possesses advantages like simplicity in processing, easy control of stoichiometry, and high solubility of dopants. For example, the solid solubility of Mg-doped STO films prepared by sol–gel is around 30%, while a much lower solid solubility was obtained for ceramics (only <1%).[24]

In our experiments, stoichiometric amounts of $Ho(NO_3)_3\cdot5H_2O$ (99.5%) and $Sr(CH_3CHOO)_3\cdot H_2O$ (99.5%) were dissolved in the solution of acetic acid and 2-methoxyethanol. After stirring, tetra-butyl titanate $Ti(OC_4H_9)_4$ (99.8%) was added into the solution. The sol was then stabilized by adding acetylacetone. The solutions were spin-coated onto $Pt/Ti/SiO_2/Si(100)$ substrates for PEC and dielectric measurements and onto quartz substrates for optical absorption

measurements. The wet films were dried at 200 °C for 1 min and then heated at 400 °C for 10 min in a silica tube. This coating process was repeated eight times to achieve the desired thickness. Finally, the films were annealed at 700 °C for 2 h in air for crystallization. The thickness of the films is about 300 nm, which was checked by a profilometer. Pt nanoparticles were coated onto the STO films using the radio frequency (RF) sputtering technique.[25] The STO films were placed parallel to the target at a distance of 60 mm and kept at room temperature. The chamber was first pumped down to 1×10^{-4} Pa, and then argon gas was introduced to reach a pressure of 1.5 Pa. Before deposition, the target was presputtered in argon for 3 min, and the RF power was set at 30 W. The amount of Pt nanoparticles was controlled by the sputtering times.

The structure of the films was analyzed by an X-ray diffraction (XRD) diffractometer (Rigaku D/MAX 2000PC). The surface morphology of the films was observed using a scanning probe microscope (NT-MDT Solver P47-PRO) operating in the contact atomic force microscope (AFM) mode. The optical absorption spectra of the films were measured by a UV/Vis/NIR spectrometer (Perkin Elmer Lambda 750). The PEC properties were measured in a conventional three-electrode cell using an electrochemical analyzer (CHI-600D). The films, a Pt foil, and an Ag/AgCl saturated calomel electrode (SCE) were used as the working, the counter, and the reference electrodes, respectively. 0.1M KOH aqueous solution was used as the electrolyte. The light source was a 300 W Xe lamp with tunable light intensity, calibrated with a Newport 1918-C photometer. For dielectric measurements, Pt dots of 0.22 mm in diameter were sputtered onto the top surface of the films through a shadow mask. The frequency-dependence of the dielectric properties was obtained using a HP4294A impedance analyzer over a frequency range of 100 Hz–2 MHz.

Figure 1(a) shows the XRD patterns of the pure and the Ho-doped STO films. All the doped films have nearly the identical crystal structure as the pure STO film (JCPDS No. 35-0734), indicating that doping up to 2.5 mol. % of Ho cations at the Sr^{2+} sites does not introduce any impurity phase. Figures 1(b)–1(e) display the AFM images of all the films, which show good uniformity and dense surface structures. The grain size of the pure STO film is about 30–50 nm. No significant change in morphology was observed after the Ho doping.
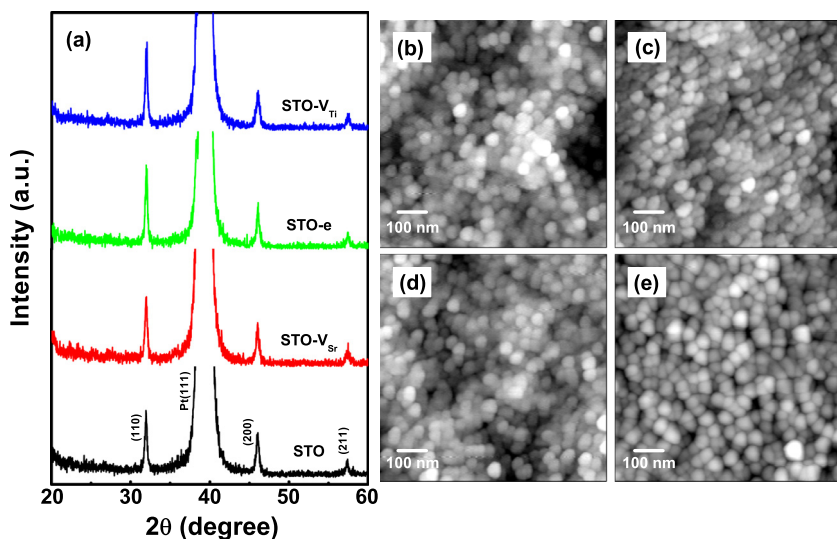

FIG. 1. (a) XRD patterns of the different STO films; AFM photographs of (b) the pure STO film; (c) the STO-V_{Sr} film; (d) the STO-V_{Ti} film; and (e) the STO-e film.

The optical absorption spectra of the pure and the Ho-doped STO films are presented in Figure 2. All the films show the intense absorption in the UV region and a steep absorption edge at around 350 nm, which implies that the absorption cannot be ascribed to the transitions of localized impurity levels but to the band-to-band transitions in the STO host. As previously reported, the valence band (VB) maximum and the conduction band (CB) minimum of STO are composed of oxygen $2p$ and titanium $3d$ orbitals,[26] respectively. Our data indicate that the band structure of Ho-doped STO films is not affected much by the orbital of Ho^{3+}. The corresponding energy band gap of the films can be estimated from the $(\alpha h\nu)^2$-$(h\nu)$ plot by extrapolating the linear portion of $(\alpha h\nu)^2$ to zero (insets of Figure 2), where α, h, and ν are the absorption coefficient, the Planck constant, and the light frequency, respectively. From the analysis, the band gap energies of the pure STO, STO-V_{Sr}, STO-e, and STO-V_{Ti} films are 3.71, 3.78, 3.80, and 3.76 eV, respectively.

Figure 3(a) shows the amperometric I-t curves of the corresponding film photoelectrodes at the zero bias measured under the modulated white light illumination. The PEC measurement is presented schematically in the inset of Figure 3(b). For all the photoelectrodes, the rise and fall of the photocurrent corresponded well to the switched illumination conditions. The photocurrent appeared promptly after the illumination and then reached a steady state. This pattern of photocurrent was highly reproducible for numerous on/off cycles of illumination. When the illumination was interrupted, the current rapidly dropped to almost zero. Upon illumination, the photocurrent jumped back to the original steady state value within a couple of seconds. The short-circuit photocurrent density of the STO photoelectrode is 1.7 $\mu A/cm^2$, which is comparable to that measured with STO nano-powder photoelectrode.[17] The photocurrent densities of STO-V_{Ti} and STO-e photoelectrodes are 3.0 and 2.4 $\mu A/cm^2$, respectively, which are 1.7 and 1.4 times higher than that of the pure STO photoelectrode. However, the photocurrent density of the STO-V_{Sr} samples is only 1.2 $\mu A/cm^2$, which is the lowest in all the samples. It is known that the photocurrent density can be affected by several factors, which convolute with each other. Among them, the band gap is the most important factor. Since no obvious change is found in all the STO films in the absorption results, such a factor cannot account for the observed difference in photocurrent. Other important factors are the crystallinity, particle size, and surface area. The XRD and AFM data, however, suggest no significant change after the Ho doping. So what is the main reason for the different PEC performances observed in this study?
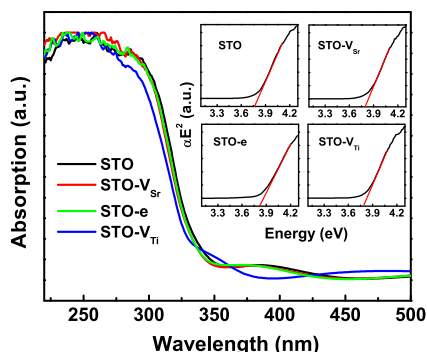

FIG. 2. UV-vis absorption spectra of the different STO films. Inset is the plots of the corresponding band gap energies.
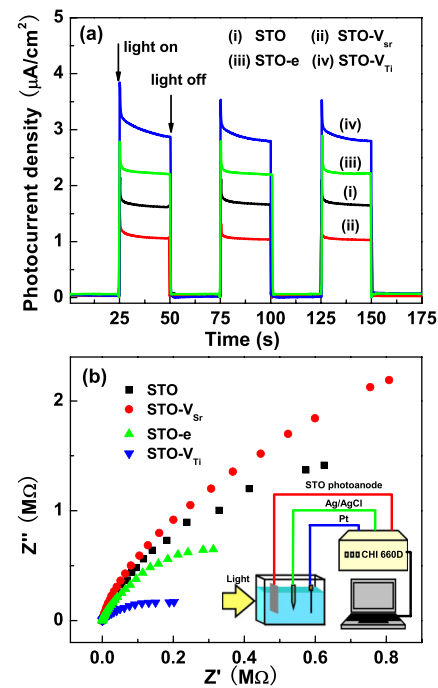

FIG. 3. (a) Photocurrent densities vs time for the different STO films at zero bias voltage. (b) EIS Nyquist plots of the different STO films. Inset: schematic diagram of the PEC measurement.

Usually, a higher photocurrent density in a PEC cell means that the photoinduced charges transfer more effectively from the photoelectrode to the counter electrode via the external circuit. In order to investigate the charge separation process, the electrochemical impedance spectroscopy (EIS) measurements without light irradiation were performed, and the data are presented in Figure 3(b). In the measurements, the Nyquist plot was scanned at an AC voltage of 10 mV with a frequency range of 0.01 Hz–10 MHz. In general, the complex impedance is usually presented as a sum of the real Z' and the imaginary Z'' components that originate from the resistance and the capacitance of the cell, respectively. A typical Nyquist plot includes a semicircle segment lying on the Z' axis followed by a straight line.[27] The semicircle region, observed at higher frequencies, corresponds to the electron-transfer-limited process, whereas the linear part at the lower frequencies represents the diffusion-limited electron-transfer process. In the case of very slow electron-transfer processes, the impedance spectrum may present only a big semicircle region. Thus, the spectrum provides information on the electron-transfer kinetics and the diffusion characteristics, and the semicircle diameter corresponds to the electron-transfer resistance. In particular, a smaller radius of the arc in the EIS spectra indicates a smaller electron transfer resistance at the surface of photoelectrodes, which usually lead to a more effective separation of photogenerated electron-hole pairs and faster interfacial charge transfer.[28] As expected, the arc radius of the EIS Nyquist plot of the samples shows opposite trend as the photocurrent density, i.e., STO-V_{Ti} < STO-e < STO < STO-V_{Sr}. Therefore, we can conclude that the PEC properties of the STO samples are strongly affected by the photogenerated charge separation, which is related to the charge compensation mechanisms.

When a semiconductor is brought into contact with a liquid, electrons will flow between them until an equilibrium is established.[29] Figure 4(a) illustrates the band energetics of a

n-type semiconductor/liquid contact in different cases. The right panel of Figure 4(a) shows the flat band potential diagram before equilibration, and the semiconductor contains a uniform distribution of charges. After the n-type semiconductor photoelectrode is in equilibrium with the liquid, the electrode will have excess positive charges at the interface, and the liquid will have excess negative charges. The band of the semiconductor will then bend upward, and the region of band bending is referred to as the depletion layer (the left panel of Figure 4(a)). During the band gap excitation, such a depletion layer assists in separating the photogenerated carriers as the electrons are driven into the bulk semiconductor and the holes to the liquid interface. Furthermore, the increase of the depletion layer width is desirable to suppress the recombination rate of the photogenerated carriers.[30] It has been known that the width of the depletion layer is proportional to the Debye length (L_D), which is given as follows:[31]

$$L_D = \left(\frac{\varepsilon_0 \varepsilon_r kT}{e^2 N_D} \right)^{1/2}, \qquad (1)$$

where ε_0 is the permittivity of free space, ε_r is the dielectric constant of the semiconductor, e is the electronic charge, k is the Boltzmann's constant, T is the absolute temperature, and N_D is the donor concentration. Figure 4(b) shows the Mott–Schottky plots of the pure and the Ho-doped STO films. All the samples exhibit positive slopes, demonstrating n-type semiconductor characteristic.[32] In the Mott-Schottky analysis,[33] the slope is inversely proportional to the effective donor concentration in the semiconductor. For the semiconductor–electrolyte interface, the capacitance (C_{cs}) of the space charge region can be described as follows:[34]

$$\frac{1}{C_{cs}} = \frac{2}{e \varepsilon_0 N_D} \left(-\Delta\phi - \frac{kT}{e} \right), \qquad (2)$$

where $\Delta\Phi$ is the difference between the applied potential and the flat-band potential. Similar to the previous report,[35] the donor concentration of the pure STO film in this study is estimated to be 8.6×10^{18} cm^{-3}. In addition, the donor concentrations are 50.8, 2.7, and 5.8×10^{18} cm^{-3} for the STO-V$_{Sr}$, STO-V$_{Ti}$, and STO-e films, respectively.

Figure 4(c) shows the dielectric properties of the pure and the Ho-doped STO films. It can be seen that the dielectric properties of all the films have a similar trend as compared to the results of photocurrent density. At 1 kHz, the dielectric constant for the pure STO film is about 220,[36] while the dielectric constants of the STO-V$_{Ti}$ and the STO-e films are higher. Again, the dielectric constant of STO-V$_{Sr}$ films is the lowest among all the samples. Since all the STO films show relatively low dielectric loss without significant difference, leakage of the samples should be excluded as the cause of the different dielectric properties. Instead, the enhanced dielectric constant can be explained as follows: When Ho^{3+} ions are incorporated at the Sr^{2+} sites in STO-V$_{Ti}$ or STO-e films, the excess positive charges can be compensated by the negative charges (titanium vacancies or conduction electrons). These opposite charges in the films are likely to form dipolar complexes due to the mutual electrostatic interaction, resulting in the increase of dielectric constant.[17,37,38]

From the results of donor concentration and dielectric constant, the Debye length of the STO-V$_{Ti}$, STO-e, STO, and STO-V$_{Sr}$ films is calculated to be 10.7, 7.7, 5.4, and 2.2 nm, respectively, as shown in Figure 4(d). Thus, we propose that different charge compensation mechanisms can result in
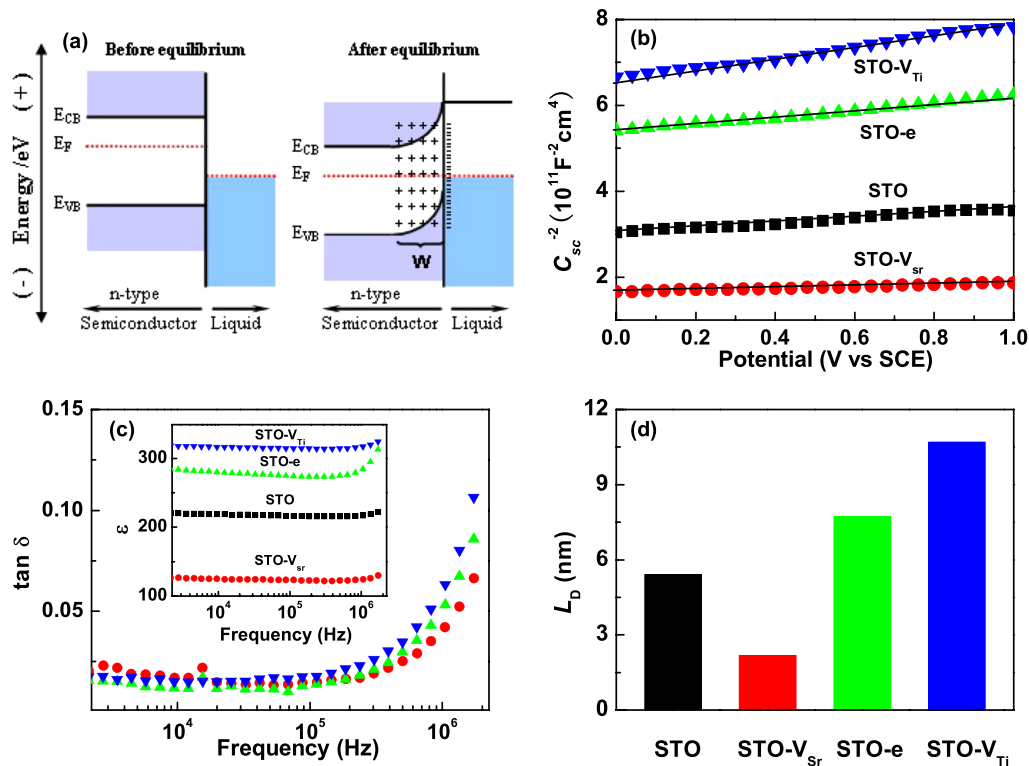

FIG. 4. (a) Schematic diagram showing the band energetic of a n-type semiconductor/liquid contact in different cases. (b) Mott–Schottky plots of the different STO films. (c) Frequency dependence of the dielectric constant and loss of the different STO films. (d) Calculation results of the Debye length of the different STO films.
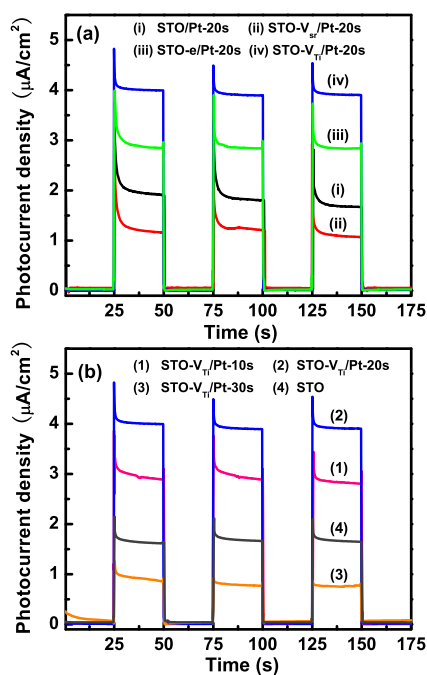
FIG. 5. (a) Photocurrent densities of all the STO films with Pt nanoparticles sputtered for 20 s. (b) Photocurrent densities of STO-V_{Ti} films with Pt nanoparticles sputtered for different times as compared to the pure STO films.

different dielectric properties of Ho-doped STO samples. A higher dielectric constant corresponds to a thicker depletion layer, increasing the number of photogenerated charge carriers which leads to an enhancement in the photocurrent density.

　　To further increase the PEC properties of the STO films, Pt nanoparticles were deposited on the surfaces of the films. Figure 5(a) shows the photocurrent densities of all the films with Pt nanoparticles sputtered for 20 s. It can be seen that all the films exhibit increased photocurrent densities. This enhancement can be attributed to the formation of Schottky barriers between Pt and STO films, and the deposited Pt nanoparticles then act as electron traps aiding the electron-hole separation.[39] Figure 5(b) shows the photocurrent densities of STO-V_{Ti} films with Pt nanoparticles sputtered for different times as compared with that of the pure STO films. The photocurrent density of the STO-V_{Ti}/Pt composite films initially increases on increasing the Pt sputtering time. The highest photocurrent density was observed for the STO-V_{Ti} films with a sputtering time of 20 s, which is 2.4 times as much as that of the pure STO films. However, as the Pt sputtering time further increases to 30 s, the photocurrent density of the sample decreases. This reduction is due to the aggregation of Pt nanoparticles, which reduces both the photon flux reaching the STO surface and the surface area of the STO film that is in direct contact with the aqueous solution.[40]

　　In conclusion, Ho^{3+} doped STO film photoelectrodes with different charge compensation mechanisms were prepared using the sol-gel method. Among all the photoelectrodes, the STO-V_{Ti} sample exhibited the highest photocurrent density, which is 1.7 times higher than that of the pure STO sample. Such an improvement in performance can be attributed to the enlarged space charge region that is related to the enhanced dielectric constant of the doped STO films. Moreover, decorating Pt nanoparticles on the film surfaces could further increase the photocurrent density, which may

be beneficial for the future application of such defect-engineered composites as photoelectrodes.

[1]K. A. Müller and H. Burkhard, Phys. Rev. B **19**, 3593 (1979).
[2]P. A. Fleury, J. F. Scott, and J. M. Worlock, Phys. Rev. Lett. **21**, 16 (1968).
[3]H. Uwe and T. Sakudo, Phys. Rev. B **13**, 271 (1976).
[4]M. Itoh, R. Wang, Y. Inaguma, T. Yamaguchi, Y. J. Shan, and T. Nakamura, Phys. Rev. Lett. **82**, 3540 (1999).
[5]J. G. Bednorz and K. A. Müller, Phys. Rev. Lett. **52**, 2289 (1984).
[6]V. V. Lemanov, E. P. Smirnova, P. P. Syrnikov, and E. A. Tarakanov, Phys. Rev. B **54**, 3151 (1996).
[7]A. Chen, Y. Zhi, P. M. Vilarinho, and J. L. Baptista, Phys. Rev. B **57**, 7403 (1998).
[8]S. M. Wrighton, B. A. Ellis, T. P. Wolczanski, L. D. Morse, B. H. Abrahamson, and D. S. Ginley, J. Am. Chem. Soc. **98**, 2774 (1976).
[9]R. Asahi, T. Morikawa, T. Ohwaki, K. Aoki, and Y. Taga, Science **293**, 269 (2001).
[10]C. Santato, M. Odziemkowski, M. Ulmann, and J. Augustynski, J. Am. Chem. Soc. **123**, 10639 (2001).
[11]I. Cesar, A. Kay, J. A. G. Martinez, and M. Gratzel, J. Am. Chem. Soc. **128**, 4582 (2006).
[12]Q. X. Jia, K. Iwashina, and A. Kudo, Proc. Natl. Acad. Sci. U.S.A. **109**, 11564 (2012).
[13]D. F. Wang, J. H. Ye, T. Kato, and T. Kimura, J. Phys. Chem. B **110**, 15824 (2006).
[14]T. K. Townsend, N. D. Browning, and F. E. Osterloh, ACS Nano **6**, 7420 (2012).
[15]H. Irie, Y. Maruyama, and K. Hashimoto, J. Phys. Chem. C **111**, 1847 (2007).
[16]K. Iwashina and A. Kudo, J. Am. Chem. Soc. **133**, 13272 (2011).
[17]J. W. Shi, J. H. Ye, L. J. Ma, S. X. Ouyang, D. W. Jing, and L. J. Guo, Chem. Eur. J. **18**, 7543 (2012).
[18]C. G. Jiang, L. Fang, M. R. Shen, F. G. Zheng, and X. L. Wu, Appl. Phys. Lett. **94**, 071110 (2009).
[19]M. J. Akhtar, Z. U. N. Akhtar, R. A. Jackson, and C. R. A. Catlow, J. Am. Ceram. Soc. **78**, 421 (1995).
[20]H. Kato and A. Kudo, J. Phys. Chem. B **106**, 5029 (2002).
[21]S. Kawasaki, K. Nakatsuji, J. Yoshinobu, F. Komori, R. Takahashi, M. Lippmaa, K. Mase, and A. Kudo, Appl. Phys. Lett. **101**, 033910 (2012).
[22]R. D. Shannon, Acta Crystallogr. **A32**, 751 (1976).
[23]A. Tkach, O. OKhay, P. M. Vilarinho, and A. L. Kholkin, J. Phys.: Condens. Matter **20**, 415224 (2008).
[24]O. Okhay, A. Y. Wu, and P. M. Vilarinho, J. Eur. Ceram. Soc. **25**, 3079 (2005).
[25]C. Ma, W. Dong, L. Fang, F. G. Zheng, M. R. Shen, and Z. L. Wang, Thin Solid Films **520**, 5727 (2012).
[26]W. Wei, Y. Dai, H. Jin, and B. B. Huang, J. Phys. D: Appl. Phys. **42**, 055401 (2009).
[27]B. Y. Chang and S. M. Park, Annu. Rev. Anal. Chem. **3**, 207 (2010).
[28]W. H. Leng, Z. Zhang, J. Q. Zhang, and C. N. Cao, J. Phys. Chem. B **109**, 15008 (2005).
[29]A. L. Linsebigler, G. Q. Lu, and J. T. Yates, Chem. Rev. **95**, 735 (1995).
[30]A. Bhardwaj, N. V. Burbure, L. Chen, A. Gamalski, and G. S. Rohrer, Chem. Mater. **22**, 3527 (2010).
[31]A. Hagfeldt and M. Gratzel, Chem. Rev. **95**, 49 (1995).
[32]K. S. Ahn, Y. Yan, S. Shet, T. Deutsch, J. Turner, and M. Al-Jassim, Appl. Phys. Lett. **91**, 231909 (2007).
[33]M. L. Zhang, W. J. Luo, Z. S. Li, T. Yu, and Z. G. Zou, Appl. Phys. Lett. **97**, 042105 (2010).
[34]E. Barsoukov and J. R. Macdonald, *Impedance Spectroscopy* (Wiley, New York, 2005).
[35]L. F. Mattheiss, Phys. Rev. B **6**, 4718 (1972).
[36]O. Okhay, A. Y. Wu, P. M. Vilarinho, and A. Tkach, Appl. Phys. Lett. **97**, 062912 (2010).
[37]M. Bassoli, M. T. Buscaglia, C. Bottino, V. Buscaglia, M. Molinari, F. Maglia, G. Parravicini, and M. Dapiaggi, J. Appl. Phys. **103**, 014104 (2008).
[38]S. A. Kelkar, P. A. Shaikh, P. Pachfule, and S. B. Ogale, Energy Environ. Sci. **5**, 5681 (2012).
[39]P. V. Kamat, J. Phys. Chem. B **106**, 7729 (2002).
[40]Z. W. Liu, W. B. Hou, P. Pavaskar, M. Aykol, and S. B. Cronin, Nano Lett. **11**, 1111 (2011).